American Mineralogist, Volume 89, pages 873–877, 2004

LETTER

A low-load, high-temperature deformation apparatus for volcanological studies

STEVEN L. QUANE,* J. K. RUSSELL, AND LORI A. KENNEDY

Igneous Petrology Laboratory, Department of Earth and Ocean Sciences, University of British Columbia, Vancouver, British Columbia, V6T 1Z4 Canada

ABSTRACT

We describe a new experimental apparatus designed to perform high-temperature, low-load (<1136 kg) deformation experiments relevant to volcanology. The apparatus accommodates samples that are up to 7.5 cm in diameter and 10 cm long, and can be used to run constant displacement rate and constant load experiments. The rig is ideal for volcanological studies because it uses experimental conditions that closely match those found in volcanic processes: temperature (25 to 1100 °C), stress (0 to >50 MPa), strain rates (10^{-6} to 10^{-2}s), and total strains of 0 to >100%. We present experimental data that show how total strain (ε_T) is distributed in pyroclastic material during welding. Our experiments use cores of analogue (glass beads) and natural (ash and pumice) materials. Coaxial deformation of the glass beads involves equal amounts of axial (ε_a; volume strain) and radial (ε_r; pure shear strain) strain until 40% strain where porosity is reduced to less than 10%. Radial strain dominates at this point. Natural materials show a different pattern because both the matrix and clasts are porous. High ratios of ε_a to ε_r are maintained until all porosity is lost ($\varepsilon_T \approx 80\%$). The implication is that welding in pumiceous pyroclastic deposits proceeds mainly by volume strain; in natural materials, pure shear strain is minimal except in special circumstances.

INTRODUCTION

Experimental methods for studying deformation processes in rocks at elevated temperatures (*T*) and high confining pressures (*P*) are well-established (e.g., Handin et al. 1972; Tullis and Tullis 1986). In particular, rock deformation presses have provided an effective means of studying mechanisms of flow in both crustal (e.g., Rutter 1993) and mantle (e.g., Karato et al. 1998) environments. Despite the importance of rheology to volcanic processes (e.g., Bagdassarov et al. 1994; Dingwell 1998), with few exceptions, these experimental techniques have not been exploited by the volcanological sciences. High-*T* deformation experiments can supply data pertinent to the formation and collapse of lava flows and domes (e.g., Spieler 2003), the transport and fragmentation of magma in conduits (Tuffen et al. 2003), or the high-*T* rheology of pyroclastic material (e.g., Boyd 1961; Friedman et al. 1963; Yagi 1966; Bierwirth 1982; Quane et al. 2002, 2003; Grunder et al. 2003).

The purpose of this paper is threefold. First, we introduce the volcanology deformation rig (VDR), which is designed for high-*T*, unconfined, low-load deformation experiments (Quane et al. 2002, 2003). The range of experimental conditions available to this apparatus make it ideal for replicating conditions associated with volcanic processes (e.g., *T*, load, strain rate). Second, we demonstrate its capacity for reproducible experiments that return real material properties. Lastly, we demonstrate the data that can be collected using a series of constant displacement rate experiments on cores of glass beads, volcanic ash, and pumice. Welding of pyroclastic deposits is an ideal process for experimental study because the conditions attending welding in natural systems, including timescales, stresses, strain rates, total strain, and temperature, are all attainable experimentally. Consequently, the experimental results can be applied directly to natural processes.

* E-mail: squane@eos.ubc.ca

EXPERIMENTAL APPARATUS

The base unit of the VDR (Fig. 1) is a LoadTrac II loadframe manufactured by Geocomp Corporation. The unit performs both constant displacement rate and constant load tests. Displacement is achieved by controlling the position of the bottom platen using an electronic stepper motor with a displacement speed range from 5×10^{-6} to 2.5×10^{-2} cm/s and measured using a built-in linear variable differential transformer (LVDT) displacement transducer with a 7.6 cm travel range and 0.00013 cm resolution. Load is measured using an S-type load cell attached to a fixed crossarm (Fig. 1). Samples can be loaded at rates from zero to 1.9 kg/s, and the maximum attainable load is 1136 kg with 0.086 kg resolution. The unit is factory calibrated for apparatus distortion during loading. An internal processor applies calibration factors for displacement (determined using a gauge block) and load (determined using a proving ring), thereby converting raw data into corrected output. Experimental output (e.g., measurements) can be collected every 0.01 s throughout the experiment. This stand-alone base unit has been modified to allow for running deformational experiments at magmatic temperatures on both consolidated and unconsolidated material.

Sample assembly

The piston and sample assembly have been constructed to facilitate high-*T* experiments (e.g., >500 up to 1100 °C; Fig. 1) on large samples. The VDR accommodates cylindrical samples having maximum diameters and lengths of 4.95 and 10 cm, respectively (Fig. 1). The upper piston is machined from Rescor 960 alumina (diameter = 4.95 cm; length = 17.75 cm) and is suspended from the load cell by a 2.5 cm length stainless steel threaded spacer. The lower piston is identical but shorter (10.16 cm in length). The alumina is insulating and retains its high compressive strengths (415 MPa) at temperatures up to 1650 °C. A tapered hole was machined through the center of the lower piston to accommodate a type-K stainless steel sheathed thermocouple. The lower piston is seated on a 15.25 cm diameter, 10 cm high, stainless steel cylinder that has a notch for the thermocouple wire.

The experiments in this study were performed on non-jacketed cores of coherent material (e.g., pumice blocks), however, the VDR can be used to experiment on unconsolidated materials, such as unsintered volcanic ash. Unconsolidated material is wrapped tightly in a jacket of 0.25 mm steel foil. Additionally, to ensure only volume strain during the experiment (e.g., no bulging) the sample can be inserted into a graphite-lubricated, type L copper tube.

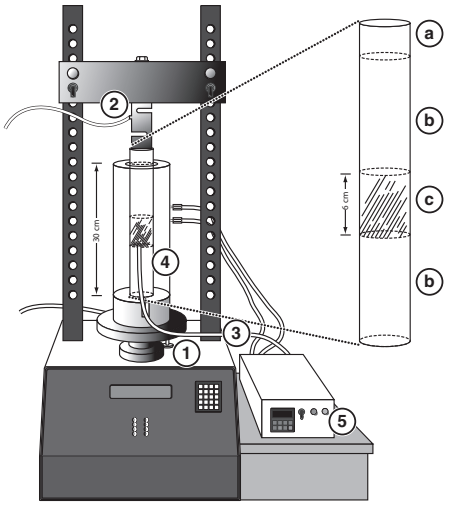

FIGURE 1. Schematic representation of the Volcanology Deformation Rig (VDR). Base unit is a Geocomp Corporation Load Trac II load frame with LVDT displacement transducer (1), and load cell with an 1136 kg limit (2). Basic load frame is modified for high-*T* experiments by adding thermocouple (3), fiber-insulated furnace (4), and temperature controller (5). The sample assembly comprises a steel spacer (a) attached to the load cell and two high temperature ceramic pistons (b) located above and below the sample (c).

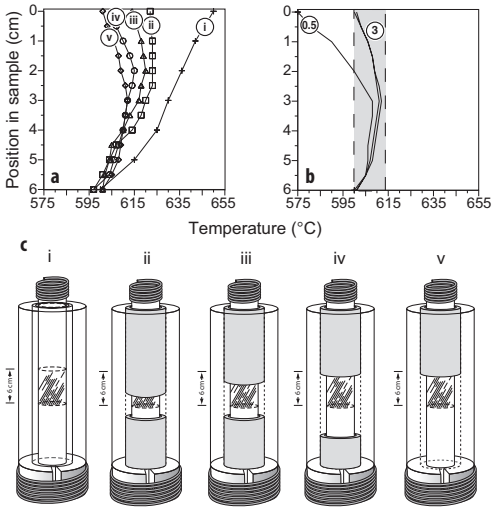

FIGURE 2. Temperature profiles (in °C) in experimental cell as a function of: (**a**) different insulation strategies (i–v; shown below), and (**b**) dwell time (see labels in hours) for insulation model v. Shading highlights the temperature profile used at the start of experiments after a dwell time of 1 hour; total temperature variation from top to bottom of sample is 12 °C. (**c**) Schematic of furnace and piston assembly to show range of insulation strategies (i–v; gray shading).

Furnace assembly

High temperatures are required if experiments are to be pertinent to volcanic processes. Temperature was attained by adding a factory built Zircar® -type FIH fiber insulated heater tube furnace to the VDR. The furnace has helically wound, Fe-Cr-Al alloy resistance wire elements embedded in a rigid body of high-temperature refractory fiber, is 30.5 cm long, and has inner and outer diameters of 7.6 and 15.25 cm, respectively. It is seated on the steel base and surrounds the lower piston, the sample and most of the upper piston (Fig. 1). The furnace generates temperatures up to 1100 °C. A K-type thermocouple connected to a Fuji PXZ-4 PID temperature controller is used to monitor and control temperature during the experiment. The basal steel cylinder and upper steel spacer are wrapped in 0.635 cm copper tubing through which tap water is run continuously to keep the load cell and LVDT at the recommended working temperatures (<60 °C).

One attribute of this experimental design is that we can run experiments on relatively large samples (e.g., 750 cm^3). Using large samples, however, raises the issue of temperature gradients within the sample during the experiment. To address this issue, we prepared a set of pumice cores with center holes drilled throughout their length. In addition to the regular VDR monitoring thermocouple (at the base of the core), a calibration thermocouple attached to an external temperature-monitoring device was inserted into the center hole. The calibration thermocouple was then moved up the center hole to map the temperature profile from the bottom to the top of the core (Fig. 2). This procedure was used to measure temperature profiles (sampled at 0.5 cm intervals) for a variety of experimental configurations and as a function of pre-experiment dwell time (0.5, 1.0, 2.0, and 3.0 h; Fig. 2).

Without insulation, convection of air causes a 40–50 °C gradient across a 6 cm core (Fig. 2; curve i). We dampened this effect by wrapping Cotronics Rescor blanket insulation around the sample assembly to completely fill the space between the assembly and inner furnace wall (Fig. 2). Temperature profiles are shown in Figure 2 for five different baffle geometries (T = 600 °C). By wrapping insulation only around the upper piston (Fig. 2a; v) we produced a symmetric temperature profile that reaches steady-state after a 1 hour dwell time, and shows a total variation of ~12 °C (Fig. 2b).

RESULTS

Data treatment

The VDR can perform isothermal experiments under the conditions of constant displacement rate or constant load. Each experiment generates a nearly continuous set of raw measurements including: time (s), load (kg), and displacement (cm) from which we compute stress (MPa), strain, and strain rate (s^{-1}). Stress (σ) is calculated from:

$$\sigma = \text{load}/\pi r^2$$

where r is the radius of the sample core. This relationship between core geometry and stress can be exploited to extend the upper and lower ranges of the VDR even though the load cell has an upper limit of 1136 kg. In natural systems, welding typically operates under stresses of <5 Mpa, however, the VDR can achieve stresses as high as ~150 MPa by using 1 cm diameter cores (Fig. 3a). We mainly used 4.4 cm diameter cores because they provide abundant material for post-experiment analysis.

Strain is calculated as:

$$\varepsilon = \Delta l/l$$

where Δl is the experimental displacement and l is the original length of the sample. The VDR allows a total displacement of 7.6 cm; this means that a wide variety of sample lengths can be used for relatively high strain experiments (Fig. 3b). A 10 cm long core, for example, can undergo 75% shortening. Most of our experiments used 6 cm length cores.

Cumulative (or incremental) strain rates are calculated from values of time and displacement:

$$\varepsilon^0 = (\Delta l/l)/\Delta t$$

where Δt is the measurement time interval.

Experimental results

Below, we explore the rheological behavior of pyroclastic materials at elevated temperatures using a set of isothermal (600 °C), constant displacement rate (5×10^{-4} cm/s) experiments. The experiments use fabricated (e.g., sintered) cores of 2 mm soda lime glass beads (see Table 1). Figure 4 shows cores and thin section images of the starting material (Fig. 4a) and run products that sustained different amounts of strain (Figs. 4b and 4c).

In these experiments on sintered glass beads, strain is manifested in several ways, including (1) reduction of core length (e.g., shortening); (2) change of core geometry (e.g., barrelling); (3) reduction of primary porosity (e.g., volume loss); and (4) deformation of original spherical beads (e.g., flattening). These indicators of strain represent the combined effects of axial strain (ε_a) accommodated by porosity loss (volume strain) and radial strain (ε_r), which conserves volume and requires geometric changes (pure shear strain). One attribute of these experiments is that independent post-experiment measurements (ϕ, Δl, r) can be used to show how strain is being accommodated (e.g., volume vs. pure shear).

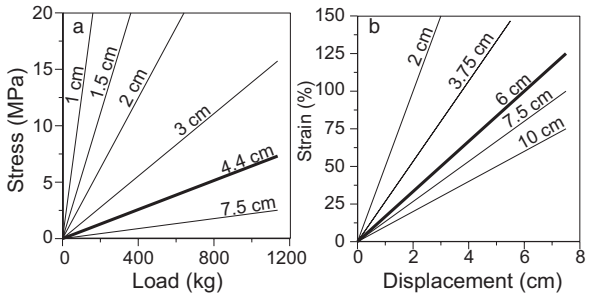

FIGURE 3. Ranges of stress and strain that are achievable with the VDR using different core geometries. (**a**) Load (kg) vs. stress (MPa) relationships showing stress limits for cores that are 1 to 7.5 cm in diameter (see labels) given the maximum load of apparatus (1136 kg). (**b**) Displacement (cm) vs. strain (%) relationships showing corresponding limits on strain for cores between 2 and 10 cm in length (see labels). The rig has a maximum displacement of 7.5 cm.

In Figure 5a, we have compared the total strain implied by machine displacement (ε_{Tm}) against the total strain based on shortening of the sample (ε_{Ts}). Here, over the full range of strain explored by these experiments ε_{Tm} is essentially equivalent to ε_{Ts} (Fig. 5a). The shortening of the sample records the total strain accumulated in the sample, however, we express this deformation in terms of two separate components. These components are calculated independently: Axial strain is calculated from:

$$\varepsilon_a = \frac{\phi_0 - \phi_l}{1 - \phi_l}$$

TABLE 1. Summary of experimental conditions used for constant displacement rate experiments illustrated in Figure 4, including temperature, displacement rate ($\Delta L/\Delta t$), and total strain (ε_T)

No.	T (°C)	$\Delta L/\Delta t$ (cm s)	ε_T	ϕ_0	ϕ_F	ε_a	ε_r
sq0804b	600	–	0	0.311	0.311	0	0
sq0717a	600	5×10^{-4}	0.377	0.331	0.123	0.22	0.21
sq0627a	600	5×10^{-4}	0.625	0.343	0.053	0.27	0.48

Note: Other parameters include the initial (ϕ_0) and final (ϕ_F) fractional porosity, as well as, the computed axial (ε_a) and radial (ε_r) strain.

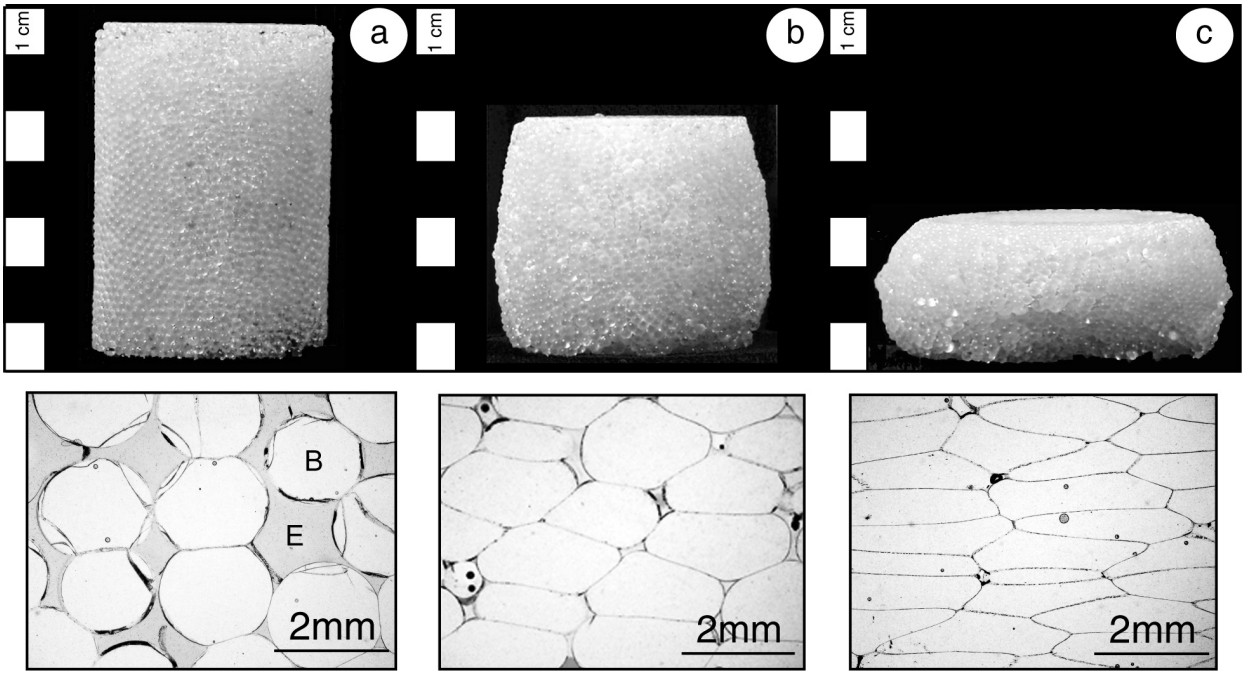

FIGURE 4. Photographs and photomicrographs of run products from constant displacement rate experiments. (**a**) Starting materials are cores made by sintering of 2 mm soda-lime glass beads. Run products are shown at (**b**) 40% and (**c**) 60% strain. Strain is accommodated during experiment by porosity loss (axial strain) and changes in core radius (radial strain). Photomicrographs show how originally spherical beads (B) progressively track strain by deforming (coaxially) to form to ellipses. Porosity, represented by colored epoxy (E) is also reduced simultaneously.

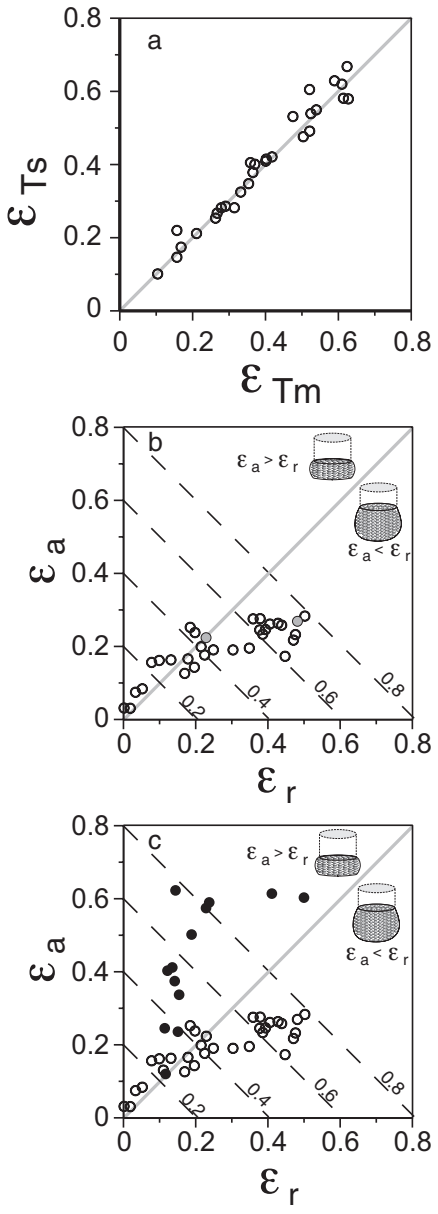

FIGURE 5. Analysis of strain in high-*T* deformation experiments of cores of glass beads, pumice, and volcanic ash. (**a**) Comparison of strain computed from machine displacement (ε_{Tm}) to strain recorded by samples as shortening (ε_{Ts}). Data are distributed evenly along 1:1 line for full range of strains (see text). (**b**) Comparison of axial strain (ε_a) and radial strain (ε_r) for experiments involving soda lime glass beads (open circles) including the 2 experiments summarized in Table 1 (solid circles). Axial strain is calculated from the reduction of porosity and represents volume strain. Radial strain is calculated from the geometry of the core (barreling) at the end of the experiment and represents pure shear strain. Dashed lines are iso-strain contours. (**c**) Comparison of axial strain (ε_a) and radial strain (ε_r) for experiments on natural materials (solid circles) and compared to data from glass beads (e.g., **b**). See text for discussion.

where ϕ_0 is the initial sample porosity and ϕ_1 the porosity of the run product determined by image analysis (Table 1). Radial strain is given by:

$$\varepsilon_r = 1 - \frac{r_0^2}{r_1^2}$$

where r_0 is the radius of the core before experiment and r_1 the mean radius of the run product. Calculated values of ε_a and ε_r for 32 experiments on glass beads performed at different experimental conditions are plotted in Figure 5b. For the analogue experiments, there is a 1:1 relationship between ε_a and ε_r until ~40–45% strain is attained. At this point porosity is reduced to ~10% and ε_r becomes dominant.

APPLICATION TO WELDING

The glass beads serve as an excellent analogue material for investigating aspects of welding processes in volcanology. The material is effective because the beads are compositionally homogeneous: they have a uniform, well-defined glass transition temperature (*T*g; 440–460 °C), and they have a regular (e.g., spherical) geometry thereby providing another strain marker. As shown in Figure 4, the spherical beads accommodate strain by flattening to form oblate spheroids. Indeed, measured values of oblateness for these strain markers fall on the theoretical curvilinear relationship for constant volume coaxial strain (Quane and Russell, in review).

In this regard, the analogue experiments do not capture the full essence of welding in pyroclastic deposits. In natural systems, starting porosities are higher (~50–75% e.g., Smith 1960; Ross and Smith 1961; Smith & Bailey 1966; Sheridan and Ragan 1976) and comprise matrix porosity as well as the porosity in individual pyroclasts. As strain accumulates, clasts will deform (flatten) but their deformation is not limited by a constant volume constraint (e.g., Sheridan and Ragan 1976; Quane and Russell in review) as is the deformation of glass beads. The consequence of this difference is shown by experiments on cores of pumiceous rhyodacite ($N = 7$) and sintered cores of rhyolite ash ($N = 6$). These data are plotted in Figure 5c. In every case, ε_a (e.g., volume strain) dominates over ε_r until very high values (~ 80%) of total strain. At this point, presumably all pore space has been lost and, thus, further strain is dominantly radial (ε_r; Fig. 5c). One implication is that welding of pyroclastic deposits is controlled by volume strain processes and, therefore, welding in pyroclastic deposits is most likely limited by porosity loss. Our welding experiments indicate that in natural systems, pure shear strain (ε_r) contributes only a minor (<10%) component to the total strain during welding as long as there is significant porosity. We suggest that pure shear strain is, in fact, not important to welding processes in most pyroclastic deposits except under extraordinary circumstances.

Pure shear strain may be important in situations where (1) the deposit's residence time in the welding window (e.g., $T > T_g$) is great relative to the average timescale of deformation, or (2) the deposit is on a substantial slope. The former situation might be realized in very thick deposits or in deposits emplaced at $T >> T_g$. Higher strain rates would result from increased load (thickness) or because of the very short relaxation timescales associated with the high emplacement temperatures (e.g., Dingwell and Webb

1990). The higher strain rates allow for attainment of near-zero porosity before the system is quenched thermally. In the remaining deformation interval, pure shear strain would dominate.

In the latter situation, where the pyroclastic deposit is on a substantial slope, the overburden load may be resolved into shear stresses that induce non-coaxial strain that is not necessarily coupled to porosity loss (e.g., pure or simple shear). Therefore, the ε_r contribution to total strain could be substantial (e.g., rheomorphism; Wolff and Wright 1981).

Conclusions

The experimental device presented here is capable of exploring a unique portion of experimental space (e.g., *T*, stress, and strain rate). The VDR provides a vehicle for exploring relationships among temperature, load, and strain, and the extent of compaction, sintering, and flattening of hot pyroclastic mixtures (e.g., ash and lapilli). Such experimental results are required to (1) constrain the mechanisms of deformation that control welding processes, and (2) develop constitutive relationships for the rheology of pyroclastic materials. This basic science is needed to address volcanological issues such as predicting the distribution of welding in ignimbrites, or establishing timescales of cooling, welding, and compaction of ignimbrites, or estimating the paleothickness of partly eroded ignimbrites.

Acknowledgments

This research was made possible by the excellent technical support from the machinists in the Department of Earth and Ocean Sciences at UBC. In particular, the authors are indebted to R. Rodway for his time, patience, and innovative spirit. We also acknowledge N. Austin and S. Israel for insightful discussions, M. Mossing for assistance with laboratory measurements, and K. Bowyer for help with illustrations. We thank C. Shaw, C. Lesher, and H. Tuffen for insightful reviews, and M. Streck and A. Grunder for directing us to the outcrops of Rattlesnake Ash. Funding derived from the University of British Columbia through a Teaching and Learning Enhancement Grant (L.A.K. and J.K.R.) and from the generous support of the Geological Society of America to SLQ via the Graduate Student Research Grants program.

References cited

Bagdassarov, N., Dingwell, D.B., and Webb, S.L. (1994). Viscoelasticity of crystal- and bubble-bearing melts. Physics of the Earth and Planetary Science Interiors, 83, 83–99.

Bierwirth, P.N. (1982) Experimental welding of volcanic ash. Bachelors Thesis, Monash University.

Boyd, F.R. (1961). Welded tuffs and flows in the Rhyolite Plateau of Yellowstone Park, Wyoming. Geological Society of America Bulletin, 72, 387–426.

Dingwell, D.B. (1998): Recent experimental progress in the physical description of silicic magma relevant to explosive volcanism. In J.S. Gilbert and R.S.J. Sparks, Eds., The Physics of Explosive Volcanic Eruptions. Geological Society, London, Special Publications, 145, 9–26.

Dingwell, D.B. and Webb, S.L. (1990) Structural relaxation in silicate melts. European Journal of Mineralogy, 2, 427–449.

Friedman, I., Long, W., and Smith, R.L. (1963) Viscosity and water content of rhyolite glass. Journal of Geophysical Research, 68, 6523–6535.

Grunder, A.L., Laporte, D., and Druitt, T.H. (2003) Experimental constraints on welding in rhyolitic ignimbrite. AGU-EUG-EGS Joint assembly, Nice, France 2003.

Handin, J., Friedman, M., Logan, J.M., Pattison, L.J., and Swolfs, H.S. (1972). Experimental folding of rocks under confining pressure; Buckling of single-layer rock beams. In H.C. Heard, I.Y. Borg, and N.L. Carter, Eds., Flow and Fracture of Rocks, Geophysical Monograph, American Geophysical Union, 16, 1–28.

Karato, S., Zhang S., Zimmerman, M.E., Daines, M.J., and Kohlstedt, D.L. (1998) Experimental studies of shear deformation of mantle materials; towards structural geology of the mantle. Pure and Applied Geophysics, 151, 589–603.

Quane, S.L., Russell, J.K., and Kennedy, L.A. (2002) The rheology of welding: experimental deformation studies. Experimental Mineralogy Petrology and Geochemistry Conference IX, 7, 86.

——— (2003) Rheology of welding: experimental constraints. AGU-EUG-EGS Joint assembly, Nice, France 2003.

Ross, R.S. and Smith, R.L., (1961) Ash-flow tuffs; their origin, geologic relations and identification. United States Geological Survey Professional Paper 366.

Rutter, E.H. (1993) Experimental rock deformation: techniques, results and applications to tectonics. Geology Today, 9, 61–65.

Sheridan, M.F. and Ragan, D.M. (1976) Compaction of ash-flow tuffs. In G.V. Chilingarian and K.H. Wolf, Eds., Compaction of coarse-grained sediments, II. Elsevier, Amsterdam, Netherlands, p. 677–717.

Smith, R.L. (1960). Ash flows. Geological Society of America Bulletin, 71, 795–842.

Smith, R.L. and Bailey, R.A. (1966). The Bandelier Tuff, a study of ash-flow eruption cycles from zoned magma chambers. Bulletin of Volcanology, 29, 83–104.

Spieler, O., Dingwell, D.B., and Alidibirov, M. (2003) Magma fragmentation speed: an experimental determination. Journal of Volcanology and Geothermal Research, 129, 109–123.

Tuffen, H., Dingwell, D.B., and Pinkerton, H. (2003) Repeated fracture and healing of silicic magma generate flow banding and earthquakes? Geology, 31, 1089–1092.

Tullis, T.E. and Tullis, J. (1986) Experimental rock deformation techniques. In Hobbs, B.E. and Heard, H.C., Eds., Mineral and Rock Deformation; laboratory studies; the Patterson Volume. Geophysical Monograph, 36, 297–324.

Wolff, J.A. and Wright, J.V. (1981) Rheomorphism of welded tuffs. Journal of Volcanology and Geothermal Research, 10, 13–34.

Yagi, K., (1966) Experimental study on pumice and obsidian. Bulletin of Volcanology, 29, 559–572.

Manuscript received October 31, 2003
Manuscript accepted January 15, 2004
Manuscript handled by Robert Dymek